ChemComm

COMMUNICATION

View Article Online
View Journal | View Issue

Cite this: *Chem. Commun.*, 2018, **54**, 13155

Received 19th August 2018,
Accepted 30th October 2018

DOI: 10.1039/c8cc06744a

rsc.li/chemcomm

Synergistic effect of bimetallic PdAu nanocrystals on oxidative alkyne homocoupling†

Zheng Chen, Rongan Shen, Chen Chen, Jinpeng Li * and Yadong Li

Bimetallic PdAu nanocrystals with different component ratios were obtained to investigate alkyne homocoupling. We found that the synergistic effect of Pd and Au plays an important role in the reaction. Alkynes with a variety of substituent groups could efficiently be converted into the corresponding 1,3-diynes through oxidative coupling.

1,3-Diynes are important building blocks in natural products, pharmaceutical intermediates and organic electronic compounds.[1–4] The straightforward method for preparing 1,3-diynes is through oxidative homocoupling of terminal alkynes developed by Glaser and Hay. Normally, the reactions are catalyzed by Cu(I) salts assisted with bases, or by catalytic systems combining palladium with copper salts in homogeneous catalysis.[5,6] However, because of the advantages of heterogeneous catalysts, like their prominent recyclability and stability, many efforts have been made to investigate efficient heterogeneous catalysts for alkyne oxidative homocoupling.[7–9] Although many achievements have been made, the catalysts usually involve very complicated synthesis processes for anchoring the organic ligands to stabilize the metal catalysts.

Metallic nanocrystals (NCs) have been widely investigated as heterogeneous catalysts for organic reactions. Van Bokhoven *et al.* investigated the catalyst performance of gold clusters for synthesizing 1,3-diynes.[10] Pu *et al.* used Pd nanoparticles as the catalyst for the same homocoupling.[11] Nevertheless, all of them need extra homogeneous additives for a continuous reaction process. Corma *et al.* showed that gold nanoparticles supported on a large variety of solids could catalyze base-free homocoupling of different alkynes with air as the terminal oxidant, but the cationic sites as the essential parts for catalyzing the process are highly limited in the clusters.[12] Bimetallic nanocrystals are emerging for modifying the properties of the monometallic materials.[13–15] Recent research studies exhibit their wide applications in heterogeneous catalysis due to the capabilities of synergistic effects between the two metals. PdAu bimetallic NCs have already been demonstrated to be efficient catalysts for other C–C coupling reactions,[16–18] whereas their performance for alkyne oxidative homocoupling has not been explored.

In recent years, our group has made great efforts to synthesize bimetallic nano-materials, and explore their growth mechanisms and catalytic properties.[19–21] We find that synergistic effects play important roles in bimetallic catalysts. In this work, we use mesoporous graphitic carbon nitride (mpg-C_3N_4) as the heterogeneous solid base to support PdAu bimetallic NCs and investigate their synergistic effects in oxidative homocoupling of terminal alkynes.[22–24]

To investigate the catalytic activity of bimetallic nanocrystals, we prepared PdAu alloys with different ratios (3 : 1, 2 : 1, 1 : 1, 1 : 2, and 1 : 3) and pure Au or Pd nanocrystals.[25] Typically, $Pd(acac)_2$ (acac = acetylacetonate) and aqueous $HAuCl_4$ were used as the precursors, and oleylamine (OAm) was used both as the solvent and the surfactant in the reaction. Stoichiometric amounts of the precursors were dissolved in OAm at 60 °C and reduced by borane-*tert*-butylamine at 80 °C. The transmission electron microscopy (TEM) images of the as-prepared NPs from Fig. 1 and Fig. S1 (ESI†) show that all stoichiometric ratios of the nanocrystals are monodispersed with the diameters of around 3–4 nm.

Fig. S2 (ESI†) shows the powder X-ray diffraction (XRD) of as-prepared bimetallic nanocrystals with different compositions, and the pure Pd and Au NPs are included as the references. The shifts of the (111) diffraction peaks from Au to Pd demonstrate the formation of the bimetallic alloy using these two elements. The detailed structures and compositions of the bimetallic alloys were characterized by the high resolution TEM (HRTEM) (Fig. 1d–f). The interfringe distance of the PdAu(1 : 1) nano-particles is about 0.233 nm, which is right between the characteristic distances of the Pd and Au (111) lattice planes, indicating the formation of the Pd–Au alloy (Fig. 1f). The energy-dispersive X-ray spectroscopy

Department of Chemistry, Tsinghua University, Beijing, 100084, P. R. China. E-mail: roclie@gmail.com

† Electronic supplementary information (ESI) available: Synthesis and experimental details, TEM, XRD and catalysis data. See DOI: 10.1039/c8cc06744a

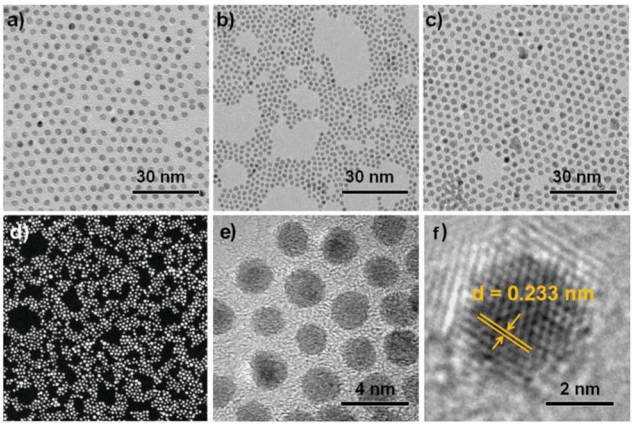

Fig. 1 TEM images of Pd NPs (a), PdAu NPs (b), and Au NPs (c); (d) high-angle annular dark-field (HAADF) STEM image of Pd_2Au nanoparticles; (e) HRTEM image of Pd_2Au nanoparticles; (f) interfringe distance measured by a single PdAu particle.

profiles support the evidence of distribution of the Pd and Au elements in the bimetallic nanocrystals (Fig. 2). As shown in Fig. 2, the line-profile analysis and EDS mapping *via* STEM-EDS of Pd_3Au reveal that the main distribution of nanoparticles is Pd (Fig. 2a and d). The surface segregated Au of Pd_3Au nanoparticles could be found. Meanwhile, Pd_2Au shows more serious surface aggregation of Au (Fig. 2b and e), which evidenced that more Au species are likely to exist at the surface.

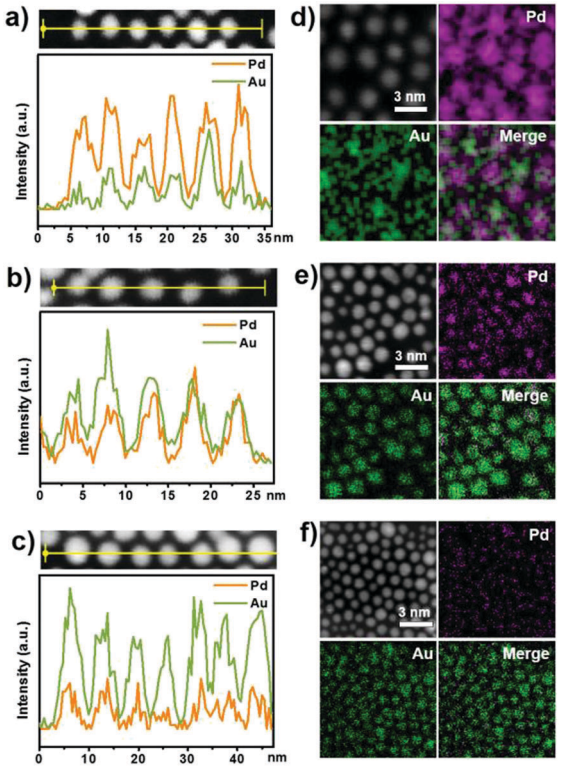

Fig. 2 Line-scanning profiles across several PdAu nanoparticles and EDX elemental mapping images by elements: (a and d) Pd_3Au, (b and e) Pd_2Au, and (c and f) PdAu.

PdAu reveals the mainly Au dispersion on the nanoparticles for the low amount of Pd species (Fig. 2c and f).

To evaluate the activity of the bimetallic catalysts, the mpg-C_3N_4 was used both as the solid-state base and the catalyst support (Fig. S3, ESI†). The mpg-C_3N_4 was synthesized using a traditional method as described previously.[26] The homo-coupling of phenylacetylene was catalyzed by PdAu/mpg-C_3N_4 in DMF at 80 °C for 12 h; meanwhile the monometallic counterparts, the mixture of them and the bare mpg-C_3N_4 support were also investigated under the same reaction conditions. Fig. 3a and Table S1 (ESI†) list the conversion ratio and selectivity of all catalysts. Fig. 3a indicates that no homo-coupling reactions are carried out with Au/mpg-C_3N_4 and the bare mpg-C_3N_4 support. Only a small amount of the product, about 2.2%, is detected in Pd/mpg-C_3N_4. The conversion is slightly increased by using a mixture of Pd and Au nanocrystals, though the conversion ratio is still less than 10%. In contrast, the bimetallic catalyst, with the metal ratio of 1 : 1, converts 41% of reactants to the final product with nearly 100% selectivity, which demonstrates the importance of the synergistic effect in bimetallic catalysts. For further understanding the relationship between the reactivity and the composition of the bimetallic catalysts, bimetallic NCs with different metal ratios were used to catalyze the homocoupling reaction. It was found that the reactivity increased when the palladium component increased. No reaction was detected when the Pd : Au ratio is 1 : 3, but the reaction is carried out when the Pd ratio increases to 1 : 2. The highest yield for the target product was found when the Pd : Au ratio changed to 2 : 1. Further increasing the Pd ratio led to a decrease in yield and selectivity.

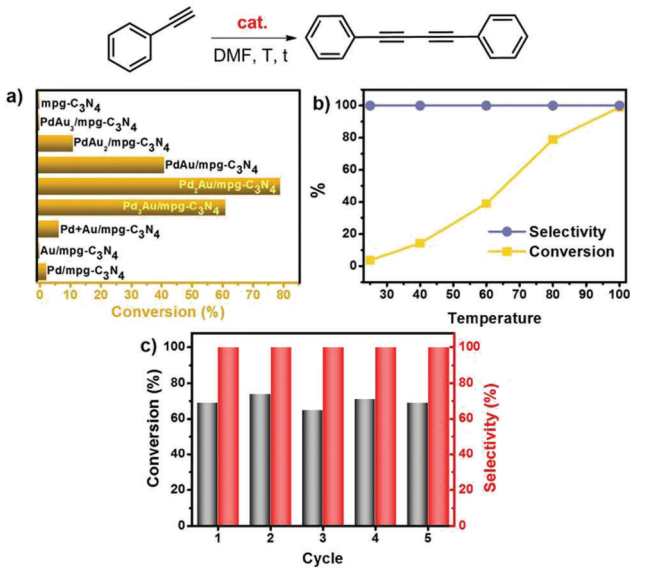

Fig. 3 (a) Catalytic results for various heterogeneous catalysts (reaction conditions: 1 mmol phenylacetylene, 5 ml DMF as a solvent, air, 80 °C, 12 hours, a 50 mg catalyst of which 2 mmol% based on the total metal is loaded on mpg-C_3N_4, the conversion and selectivity are determined by GC using biphenyl as an internal standard); (b) the conversion and selectivity at different temperatures; (c) the recycling ability of PdAu/mpg-C_3N_4 for oxidative homocoupling of phenylacetylene within 8 h at 100 °C.

The conversion increased with elevated temperature (Fig. 3b) and complete conversion with 100% selectivity was obtained at 100 °C within 12 h. Based on the kinetic study on the percentage of phenylacetylene and 1,4-diphenylbutadiyne, the reaction could be finished in 10.5 h (Fig. S4, ESI†). The catalyst is recycled and reused in the oxidative homocoupling 5 times to study the reusability of the Pd–Au bimetallic catalyst (Fig. 3c). It is easy to collect the nano-catalyst by hot filtration from the liquid phase of the reaction mixture. The cycling experiments were executed at 100 °C with 8 h as the reaction time. From Fig. 3c we can find that the yield and selectivity of the product do not change significantly during these 5 cycles, which indicates the durability of the catalyst. The resulting solution was analyzed *via* ICP-MS. Only a trace amount of palladium was leached to the solutions, but the solution cannot further catalyze the homocoupling reaction. These results clearly demonstrate that the reaction is completely catalyzed by the heterogeneous Pd–Au catalyst. The spent $Pd_2Au/mpg\text{-}C_3N_4$ catalyst after five cycles was characterized by TEM and XRD (Fig. S5 and S6, ESI†). $PdAu/mpg\text{-}C_3N_4$ showed basically no change whatever the dispersion on $mpg\text{-}C_3N_4$ or the crystal structure, which evidenced the stability of bimetallic PdAu catalysts in phenylacetylene homocoupling reactions.

The experiment results indicate that $Pd/mpg\text{-}C_3N_4$ can carry out the reaction without any additives, however, to further enhance the activity of the Pd particles, bases or organic ligands are needed to generate Pd cation species to react with the alkyne molecules that undergo reductive elimination leading to the diyne products and Pd(0).[27] In contrast, in the bimetallic PdAu nanocrystals, charge migration occurs from the Pd atoms to the nearest Au atoms to generate positive Pd sites for promoting reductive elimination. This synergistic effect exhibits the advantage of the bimetallic Pd–Au alloy as an effective heterogeneous catalyst for C–C homocoupling. This mechanism is further proved *via* X-ray photoelectron spectroscopy (XPS). As shown in Fig. 4a, the binding energies of Pd $3d_{5/2}$ and $3d_{3/2}$ peaks of $Pd/mpg\text{-}C_3N_4$ located at 335.4 eV and 341.7 eV are assigned to Pd(0), and the peaks at 337.9 eV and 343.0 eV are assigned to Pd(II) which are the Pd species interacting with nitrogen of $mpg\text{-}C_3N_4$ on the surface. The Pd $3d_{5/2}$ and $3d_{3/2}$ peaks of $PdAu/mpg\text{-}C_3N_4$ are located at 336.2 eV and 341.6 eV which shows the partial positive charge in PdAu particles. By comparison, the Au $4f_{7/2}$ and Au $4f_{5/2}$ peaks of PdAu are shifted obviously to the lower side in binding energy (Fig. 4b). This tendency indicates that the Au atoms gained electrons from Pd atoms by alloying interaction. For better understanding the importance of the alloy composition in catalysis, we also investigated the charge states in all ratios *via* XPS. It is clear that increasing the Pd ratio will increase the charge separation at first, and this can be attributed to more Pd atoms appearing on the surface to interact with Au, and the reactivity is also enhanced from our experiments (Fig. S7, ESI†). However, when the ratio increased to Pd_3Au, the surface is dominantly covered by Pd atoms which is proved by EDS mapping. In this case the buried Au atoms cannot interact with Pd atoms effectively, so the charge migration is inhibited. All these evidences prove that the electronic poor states of Pd atoms and the surface states in PdAu may play a crucial role in the activation of C≡C–H bonds and O_2, thus leading to high activity.

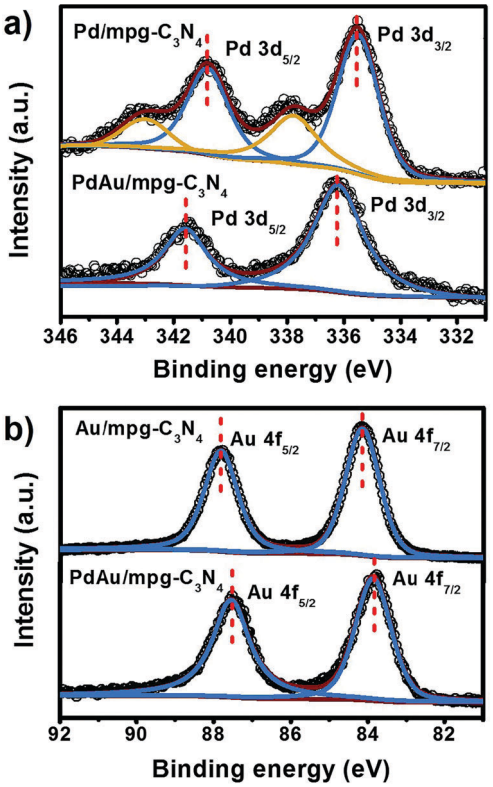

Fig. 4 XPS spectra of $Pd_2Au/mpg\text{-}C_3N_4$ compared with $Pd/mpg\text{-}C_3N_4$ (a) and $Au/mpg\text{-}C_3N_4$ (b).

For understanding the general applicability of the catalysts, we investigated the scope of homocoupling with different substrates (Table 1). The halogen substituted phenylacetylenes give relatively high yields (>90%) with the substitution being in the para or meta positions (entries 2–4). The yield decreases a little (~89%) in the presence of a strong electron withdrawing group like the nitro-group (entry 5). When the electron donating group is used as the substitution group, the yields decreases

Table 1 Scope of $Pd_2Au/mpg\text{-}C_3N_4$ catalyzed oxidative alkyne homocoupling

Entry[a]	R-	Time (h)	Con.[b] (%)	Sel.[b] (%)
1	H	12	99	100
2	*p*-Cl	12	95	100
3	*p*-Br	12	96	100
4	*m*-F	12	91	100
5	*p*-NO_2	14	89	100
6	*p*-MeO	16	79	100
7	*m*-NH_2	16	71	100
8	1-Heptene	20	89	100

[a] Reaction conditions: 1 mmol alkyne, 5 ml DMF as a solvent, air, 100 °C, and 50 mg $Pd_2Au/mpg\text{-}C_3N_4$. [b] The conversion and selectivity are determined by GC using biphenyl as an internal standard.

to less than 80% (entries 6 and 7). An alkyl terminal alkyne like 1-heptyne also gives a relatively high yield (~89%) in the homocoupling reaction (entry 8). All reactions give a full selectivity without any byproducts.

In conclusion, we systematically studied the catalytic characteristics of the bimetallic PdAu nanocrystals in alkyne oxidative homocoupling reactions. The synergistic effect of the bimetallic alloy has been observed through our investigation. This effect can be attributed to the charge migration from the Pd atoms to Au atoms. The bimetallic nano-catalysts showed highly efficient activity in homocoupling of terminal alkynes under mild conditions. These heterogeneous catalysts also showed high stability and reusability over a number of cycles. All these results indicate that our bimetallic Pd can be effective heterogeneous catalysts for the C–C homocoupling reactions for further industrial applications.

This work was supported by the National Key R&D Program of China (2016YFA0202801 and 2017YFA0700101), the National Natural Science Foundation of China (21573119, 21590792, 21521091, 21390393, and U1463202) and the China Postdoctoral Science Foundation (2018M631444).

Conflicts of interest

There are no conflicts to declare.

Notes and references

1 A. L. K. Shi Shun and R. R. Tykwinski, *Angew. Chem., Int. Ed.*, 2006, **45**, 1034–1057.
2 J. S. Lampkowski, D. M. Uthappa, J. F. Halonski, J. C. Maza and D. D. Young, *J. Org. Chem.*, 2016, **81**, 12520–12524.
3 F. Diederich, P. J. Stang and R. R. Tykwinski, *Acetylene Chemistry: chemistry, biology and material science*, Wiley-VCH, 2005.
4 B. J. Eckstein, F. S. Melkonyan, N. Zhou, E. F. Manley, J. Smith, A. Timalsina, R. P. H. Chang, L. X. Chen, A. Facchetti and T. J. Marks, *Macromolecules*, 2017, **50**, 1430–1441.
5 J. Jover, P. Spuhler, L. Zhao, C. McArdle and F. Maseras, *Catal. Sci. Technol.*, 2014, **4**, 4200–4209.
6 S. T. Aziz and R. U. Islam, *Catal. Lett.*, 2018, **148**, 205–213.
7 T. Oishi, K. Yamaguchi and N. Mizuno, *ACS Catal.*, 2011, **1**, 1351–1354.
8 F. Alonso and M. Yus, *ACS Catal.*, 2012, **2**, 1441–1451.
9 N. Orozco, G. Kyriakou, S. K. Beaumont, J. Fernandez Sanz, J. P. Holgado, M. J. Taylor, J. P. Espinós, A. M. Márquez, D. J. Watson, A. R. Gonzalez-Elipe and R. M. Lambert, *ACS Catal.*, 2017, **7**, 3113–3120.
10 B. Vilhanová, J. Václavík, L. Artiglia, M. Ranocchiari, A. Togni and J. A. van Bokhoven, *ACS Catal.*, 2017, **7**, 3414–3418.
11 H. Li, M. Yang and Q. Pu, *Microporous Mesoporous Mater.*, 2012, **148**, 166–173.
12 M. Boronat, S. Laursen, A. Leyva-Pérez, J. Oliver-Meseguer, D. Combita and A. Corma, *J. Catal.*, 2014, **315**, 6–14.
13 C.-H. Liu, R.-H. Liu, Q.-J. Sun, J.-B. Chang, X. Gao, Y. Liu, S.-T. Lee, Z.-H. Kang and S.-D. Wang, *Nanoscale*, 2015, **7**, 6356–6362.
14 J. Jover, M. García-Ratés and N. López, *ACS Catal.*, 2016, **6**, 4135–4143.
15 H. Yang, S. J. Bradley, A. Chan, G. I. N. Waterhouse, T. Nann, P. E. Kruger and S. G. Telfer, *J. Am. Chem. Soc.*, 2016, **138**, 11872–11881.
16 R. N. Dhital, C. Kamonsatikul, E. Somsook, K. Bobuatong, M. Ehara, S. Karanjit and H. Sakurai, *J. Am. Chem. Soc.*, 2012, **134**, 20250–20253.
17 S. Zhang, C. Chang, Z. Huang, Y. Ma, W. Gao, J. Li and Y. Qu, *ACS Catal.*, 2015, **5**, 6481–6488.
18 Z.-J. Wang, X. Wang, J.-J. Lv, J.-J. Feng, X. Xu, A.-J. Wang and Z. Liang, *New J. Chem.*, 2017, **41**, 3894–3899.
19 W. Wang, D. Wang, X. Liu, Q. Peng and Y. Li, *Chem. Commun.*, 2013, **49**, 2903–2905.
20 Y. Wu, D. Wang and Y. Li, *Chem. Soc. Rev.*, 2014, **43**, 2112–2124.
21 W. Jia, Y. Wu, Y. Chen, D. He, J. Li, Y. Wang, Z. Wang, W. Zhu, C. Chen, Q. Peng, D. Wang and Y. Li, *Nano Res.*, 2016, **9**, 584–592.
22 F. Goettmann, A. Fischer, M. Antonietti and A. Thomas, *Angew. Chem., Int. Ed.*, 2006, **45**, 4467–4471.
23 F. Su, M. Antonietti and X. Wang, *Catal. Sci. Technol.*, 2012, **2**, 1005.
24 J. Zhu, P. Xiao, H. Li and S. A. C. Carabineiro, *ACS Appl. Mater. Interfaces*, 2014, **6**, 16449–16465.
25 Z. Chen, S. Wang, C. Lian, Y. Liu, D. Wang, C. Chen, Q. Peng and Y. Li, *Chem. – Asian J.*, 2016, **11**, 351–355.
26 F. Su, S. C. Mathew, G. Lipner, X. Fu, M. Antonietti, S. Blechert and X. Wang, *J. Am. Chem. Soc.*, 2010, **132**, 16299–16301.
27 A. Toledo, I. Funes-Ardoiz, F. Maseras and A. C. Albéniz, *ACS Catal.*, 2018, **8**, 7495–7506.

